Structural and electronic properties of $PbTiO_3/SrTiO_3$ superlattices from first principles

Mingqiang Gu,[1] Jianli Wang,[2] Q. Y. Xie,[1] and X. S. Wu[1,3,*]

[1]*Nanjing National Laboratory of Microstructures, Laboratory of Solid State Microstructures, Department of Physics, Nanjing University, Nanjing 210093, China*

[2]*Department of Physics, China University of Mining and Technology, Xuzhou 221008, China*

[3]*SSRF, Institute of Shanghai Applied Physics, CAS, Shanghai 201204, China*

(Received 21 January 2010; revised manuscript received 3 June 2010; published 5 October 2010)

The interfacial structure, stability, electric polarization, and electronic properties for $PbTiO_3/SrTiO_3$ (PTO/STO) superlattice are studied by first-principles calculations. Based on the work of separation for different stacking interface configurations, including stoichiometric normal stacking interface, Ruddlesden-Popper-type interface, Magneli-type interface and interfaces with a TiO_2 inserted layer, the normal stacking interface is found to be the most stable one. Due to the charge redistribution at the interface, there are alternative appearances of *n*- and *p*-type interfaces in polar PTO/STO system driven by the internal electric field. The magnitude of charge at the interface is evaluated with a simple capacitor plates model.

DOI: 10.1103/PhysRevB.82.134102 PACS number(s): 77.84.−s, 68.35.Ct, 73.20.−r, 73.21.Cd

I. INTRODUCTION

Perovskite ferroelectric (FE) material is a topic of robust studies due to its potential applications in electronic industry[1,2] and the necessity of the fundamental comprehension of the underlying mechanism.[3–6] Crystals such as $BaZrO_3$, $BaTiO_3$ (BTO), $PbZrO_3$, and $PbTiO_3$ (PTO) were investigated in detail in the past, especially around the FE related effects such as dipole orientation under in-plane strain,[7] piezoelectric-ferroelectric relaxor coeffect,[8] etc.

Perovskites in the form of films and superlattice have relatively large area of surface and interface which contribute to dramatic distinct electronic and magnetic properties from the bulk materials. Therefore ferroelectricity in these structures is accompanied with interesting phenomena. Recently the improper FE behavior was presented in $SrTiO_3$ (STO)/PTO superlattice systems due to the rotational distortions.[6] This multilayer exhibits a very large dielectric constant (~600), which suggests important application prospect of this material. Many works have been carried out to simulate the electronic structure, surface reconstruction, domain properties, and FE mechanism of PTO,[9–12] and character of STO/PTO superlattice.[5,13,14] Most recently Nakhmanson and Naumov investigated artificial perovskite structure $PbSr_2Ti_2O_7$ with two Ruddlesden-Popper (RP) interfaces with first-principles calculations and noticed a Goldstone-type vibration state, which enriched the physics in such FE system.[15]

However, for different combination of atomic layers at the interfaces, it is still void of the interface stability, which is important and necessary for the successful design of a heterostructure. In the present work the stability and the polarization behavior for different stacking configurations of SrO, TiO_2, and PbO layers are investigated based on the *ab initio* calculations. Besides the normal stacking, which consists of stoichiometric interfaces, the supercells with RP homologous structure,[16,17] Magneli structure[18] and superlattices with TiO_2 inserted layers[19–22] at the interface are also considered.

The improper ferroelectricity resulting from couple of FE distortion with rotation of the TiO_6 octahedra, i.e., the antiferrodistortive modes, has been fully discussed by Bousquet *et al.*[6] They found that the improper ferroelectricity is significant as the repeating period of the superlattice is short enough (the repetition period approximates 1/1 or 3/2 for n_{STO}/n_{PTO}). In the present, we constrain our present simulation to refer only to the FE out-of-plane distortion.

II. METHODOLOGY

A. Simulation details

Structural and electronic properties of the superlattice system are simulated utilizing the first-principles calculations with the Vienna *ab initio* simulation package (VASP).[23] The conjugate gradient technique[24] is employed to treat the electron wave functions. PAW method of Blöchl, which is implemented in VASP,[25,26] is used to treat the core electrons. As suggested in previous literatures[27–30] that Perdew-Burke-Ernzerhof (PBE) functional[31] gives poor description for this FE system by overestimating the tetragonality and the polarization, local-density approximation is used to treat the exchange and correlation energy of the electrons. O $2s2p$, Ti $3s3p4s3d$, Sr $4s4p5s$, and Pb $5d6s6p$ states are included as valence levels.

The precision in the calculation is achieved by increasing the cutoff energy to 500 eV. In the calculations, the density of the Monkhorst-Pack *k*-point mesh[32] is $(8\times8\times1)$ for the $[PTO]_4/[STO]_4$ superlattice, $(9\times9\times1)$ for the RP and Magneli type structures, and $(10\times10\times1)$ for the TiO_2-inserted superlattices, which yields a numerical accuracy within 1 meV of the total-energy differences compared to a denser *k*-point grid during the test procedure. When calculating the work of separation, a vacuum space with four times the length of lattice constant (~12 Å) is used to prevent interaction between slabs. Test calculations show that the results are well converged.

Before starting the calculations for the superlattices, we optimize the bulk lattice constant of STO and PTO at first. The results of 3.864 Å for STO and 3.894 Å for paraelectric (PE) PTO bulk material are in reasonable agreement with those of the previous experiment[33,34] and theory.[21,28] Besides,

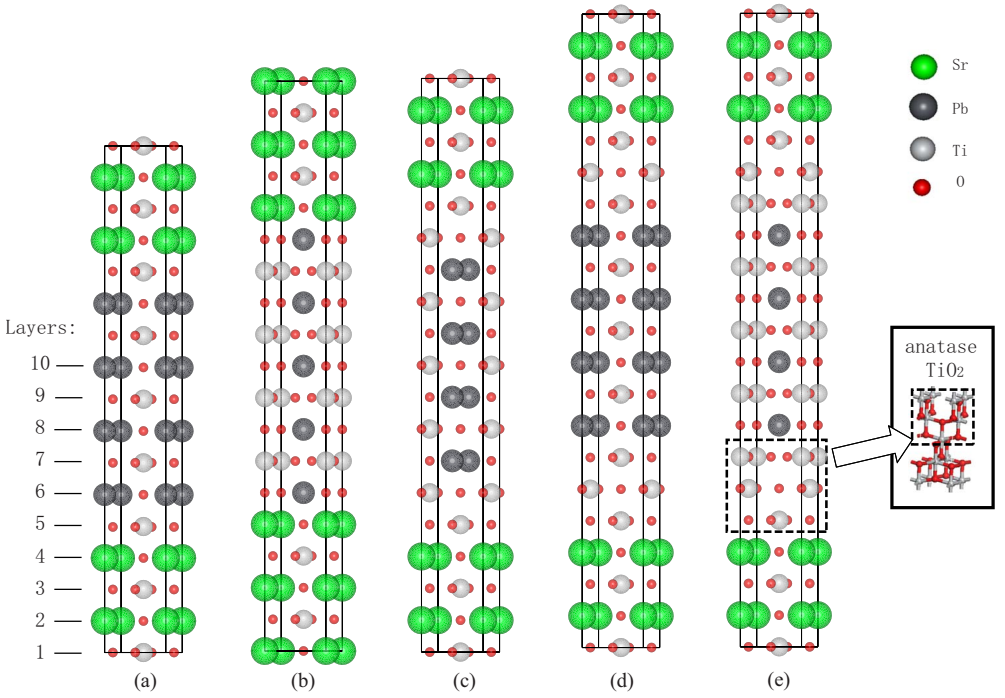

FIG. 1. (Color online) Supercell models of PTO/STO superlattices with various stacking orders (a) $[PTO]_4/[STO]_4$; (b) RP type; (c) Magneli type; (d) and (e), two kinds of TiO_2-inserted superlattices.

results of lattice constant a and the tetragonality ratio c/a for tetragonal PTO come out to be 3.870 Å and 1.04. These theoretical lattice constants will be used in the following calculations.

B. Supercell models

To trace the interface structures and electronic properties for the PTO/STO superlattices, supercells are constructed during the calculations. The growth direction of the supercells is supposed parallel to the vertical z direction. We construct possible interfaces between STO and PTO, and check the interface stabilities and their electronic properties for all kinds of stacking of the supercells. Figure 1(a) shows the stacking sequence containing four STO and four PTO unit cells in one supercell, where the regular stacking of AO and TiO_2 is not disturbed at the interface. Abnormal stacking sequences are also shown in Figs. 1(b) and 1(c). The model in (b) shows the situation with the interface of PbO and SrO. This model is often studied in perovskite interface,[35–38] which is known as RP-type defect. Figure 1(c) shows the interface geometry with two TiO_2 layers, which is known as a Magneli-type planar defect. Experimental investigation has shown that STO reconstructed surface with double TiO_2 layers[19] is available. TiO_2 adlayer may insert at the interface under high chemical potential of TiO_2. If the ad-TiO_2 layer occurs in the normal stacking, it yields a Magneli-type interface. If it appears in the Magneli structure, two new structures are formed, see in Figs. 1(d) and 1(e). Both structures have two Magneli defects at the interface while one denoted as xx (toward the same direction) and the other, xy (oriented normally). These two supercells have the same chemical formula as $Sr_4Ti_6O_{16}/Pb_4Ti_6O_{16}$.

To test the availability of different interfacial stacking cases, we first inspect the surface termination of the original STO and PTO materials. Perovskite titanates are composed of alternative AO (A=Sr or Pb) and TiO_2 planes, which would be the probable semiterminate surface in the growing process and finally affect the composition of the interface of the supercell. Our previous study[22] showed that both of SrO and TiO_2 terminated surfaces in STO are available. Here with similar process estimating the surface grand potentials as functions of the chemical potential[39] of PbO, we build two slabs containing eleven atomic layers with PbO and TiO_2 as surface termination, individually. Both PbO and TiO_2 terminated surfaces are checked to be available for PTO (see Fig. 2), which is in agreement with Zhang *et al.*[11] Therefore the consideration of different interfaces is rational.

III. RESULTS AND DISCUSSIONS

A. Structure and relaxation properties

To relax the superlattice, the proper choice of the in-plane lattice constant is an important issue for superlattice geometries. The most common choice is the constrained parameter to that of some substrate. However, considering that the RP (Magneli) structure brings planar shift along [1/2, 1/2, 0] ([1/2, 0, 0]) to the interface, an intuitionistic way to examine the relevant strain is relaxing the in-plane constant to release the induced stress. Hence we allow the in-plane lattice constant to relax, neglecting the substrate effect. The following results in tables and figures are given under such zero stress condition unless specified otherwise. We also carry out calculations with the in-plane lattice constant constrained (epitaxially strained condition) to that of STO, i.e., 3.864 Å.

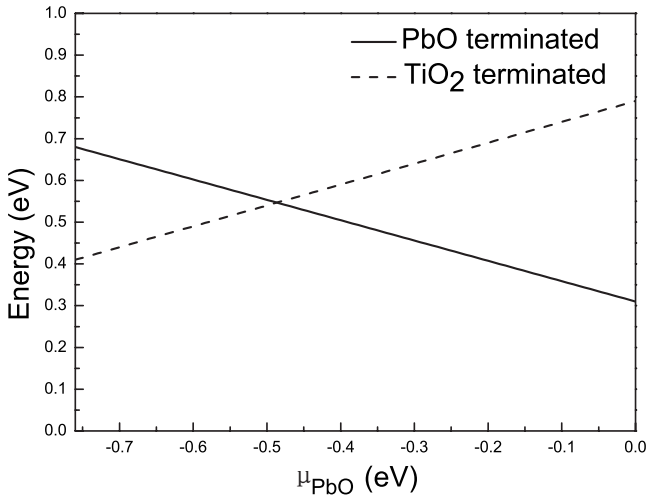

FIG. 2. Surface grand potentials of PbO- and TiO_2-terminated PTO as a function of μ_{PbO}.

With a constrained in-plane constant, strain energy yields a higher total energy, by ~0.02 eV higher than that of the structure relaxed under zero stress condition. We will make some further comparison between this two conditions in the following text.

As indicated previously, we neglect the in-plane rotation of oxygen octahedra during relaxation process since our supercell models are relatively large[6] and improper ferroelectricity effects could be negligible. Hence the in-plane coordination of the ions keeps fixed and the structures are fully relaxed along z direction.

To make sure that the symmetry breaking for FE state is spontaneous, all the slabs have access to a PE state with perfect inversion symmetry. The corresponding values of lattice parameters for these supercells are presented in Table I. Due to a shift along [1/2,0,0] direction brought by the Magneli defect, asymmetry is induced to the supercell, so the supercell has an orthorhombic structure. It can be seen that the Magneli supercell expands along the direction parallel to the shift direction while shrinks prominently in the orthogonal direction.

TABLE I. Calculated in-plane lattice constants (a and b) and polarization (P) for different supercells, given both for paraelectric (PE) and ferroelectric (FE) phase. Values in parenthesis are calculated with fixed in-plane lattice constant.

	PE phase		FE phase
	a (Å)	b (Å)	P (C/m^2)
STO	3.86		
PTO	3.89		0.762
$[PTO]_4/[STO]_4$	3.87		0.290 (0.301)
RP type	3.87		0.007 (0.005)
Magneli	3.88	3.85	0.012 (0.009)
xx	3.92	3.81	0.243 (0.222)
xy	3.85	3.86	0.011 (0.009)

The relaxed structures for normal, RP type and Magneli type interfaces are summarized in Table II. Parameters listed in Table II are schematically illustrated in Fig. 3. Let $\delta_i(C)$ and $\delta_i(O)$ $[\delta_i(O)=[\delta_i(O_1)+\delta_i(O_2)]/2$ for the TiO_2 plane] be the displacements of cation and oxygen, respectively. The displacement of the atomic plane is defined as the averaged displacements, i.e., $\delta_i=[\delta_i(C)+\delta_i(O)]/2$. The interplanar distance ξ_{i-j} between the ith and jth planes is $\xi_{i-j}=|\delta_i-\delta_j|$, which is compared with that of the ideal cubic phase STO and PTO bulk structures. We also define the rumpling η_i as the amplitude of the relative displacements between cation and oxygens, $\eta_i=\delta_i(C)-\delta_i(O)$.

Since the PE supercells are symmetric along z axis, it is sufficient to investigate only the lower half. In the first case [Fig. 1(a)] the variation in distance between layers is less significant since the interface keeps consecutive perovskite structure. The continuity of the structure geometry in the gross preserves the bonding environment of every atom. In accordance with the small quantity of plane relaxation, the rumpling is much smaller than that of the other two structures, not exceeding 0.05 Å. With dramatic deviation from general chemical formula of ABO_3, RP, and Magneli structures demonstrate severe relaxation at the interface. Superlattice with RP defect is under a ruffle of ~0.16 Å at the interface, and the PbO and SrO planes repulse from each other by more than 0.5 Å. The interplanar distances increase or decrease alternatively, indicating that the AO planes tend to be off the interface while the TiO_2 planes try to reduce this trend and stabilize the interface. The rumpling suffered by the Magneli-type interface seems not so remarkable. However, by noticing that there are two nonequivalent oxygens at the TiO_2 planes in Magneli case which relax toward the reverse directions, and the rumpling parameter in the table reflects the distance between centers of cation and the oxygen(s) at a single layer. If we turn to the common acceptation of rumpling, i.e., distance between the highest and lowest position, the actual rumpling has been underestimated in Magneli case. Actually it has the most rugged interface, with a vertical distance of more than 0.38 Å between two oxygens at the interface.

We examine the variation in vertical distances (not shown here) between two metal cations or oxygens at adjacent layers, that is, d_{ij} in Fig. 3. Distances between cations in the superlattice with RP defect increase or decrease alternatively while oxygens repulse from each others through out the whole slab. There exists the most severe discrepancy from ideal position at the RP interface, with a repulsion of 0.68 Å between cations, by more than 17% of the lattice parameter. Pb and Sr cations at the RP interface detach from each other due to electrostatic repulsion. In Magneli model both oxygens and cations oscillate around their ideal position from layer to layer. Sharing an edge, the two TiO_6 octahedra at the interface get contact with each other. It causes large and oppositely directed relaxations of oxygens in the two TiO_2 planes. Two center titanium cations also represent a repulsive trend. However, with increasing distance from the interface, the influence of both the RP and Magneli interfaces weakens very quickly. From the second plane off the interface, the interplanar distances become bulklike. This is well known as the "locality principle" of interface effects in perovskite systems.[40]

TABLE II. Variation in interplanar distances $\Delta\xi_{i-j}$ and rumpling η_i (both in angstrom) for different superlattices, where $\Delta\xi_{i-j}=\xi_{i-j}-\xi_{i-j}^{ideal}$, ξ_{i-j}^{ideal} is the interplanar distances of ideal bulk perovskite, (STO, PTO, or the average value at the interface).

PE phase			
Layer	Normal	RP	Magneli
	$\Delta\xi_{i-j}$		
1–2	0.001	0.007	0.007
2–3	−0.002	−0.014	0.002
3–4	−0.002	0.032	0.019
4–5	−0.023	−0.081	−0.034
5–6	0.027	0.514	0.268
6–7	0.004	−0.063	−0.021
7–8	0.004	0.044	0.035
8–9	0.001	−0.018	0.001
9–10		0.008	0.013
	η_i		
1	0.000	0.000	0.000
2	−0.001	0.005	0.003
3	0.001	−0.029	−0.004
4	0.001	0.029	0.025
5	0.027	−0.168	−0.016
6	−0.001	0.156	0.038
7	0.000	−0.037	−0.033
8	−0.001	0.033	0.007
9	0.000	−0.008	−0.007
10		0.000	0.000

FE Phase			
Layer	Normal	RP	Magneli
	η_i		
1	0.117	0.005	0.007
2	0.109	0.009	0.016
3	0.118	−0.027	−0.002
4	0.107	0.038	0.041
5	0.142	−0.153	−0.033
6	0.117	0.170	0.022
7	0.111	−0.027	−0.020
8	0.122	0.031	0.012
9	0.110	−0.001	0.001
10	0.123	0.003	0.007
11	0.109	0.007	0.010
12	0.123	−0.025	0.003
13	0.085	0.031	0.032
14	0.112	−0.165	−0.010
15	0.116	0.163	0.044
16	0.109	−0.034	−0.023
17		0.037	0.014
18		−0.006	0.001

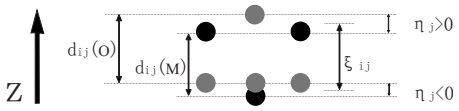

FIG. 3. Schematic illustration of the layer relaxation and the definition of parameters in Table II. Metal and oxygen ions are marked as black and gray circles, respectively.

The rumpling parameters for the polar phase are also presented. It is evident that in this case all the rumpling of the atomic layer is of the same sign for the normal stacking model, which indicates that the polarization is more or less consistent throughout the structure. This can be paraphrased as the minimization of the total electrostatic energy.[41] Other works[7,13,14] also substantiate such qualitative uniformity of local polarization of layers in PTO, BTO, and STO superlattice systems. Here the polarized rumpling caused by ferroelectricity is about 0.1 Å, larger than that in PE phase induced by interface. However, with the significant discrepancy from normal stacking at the interfaces, the RP and Magneli-type supercells do not show such consistency. The scale of ruffle caused by interface, which is nonpolarized, is much larger than that of polarized rumpling. It is recognizable that the continuity of Ti-O chains is significant to FE polarization. These chains are broken at the interface. Accordingly, the ferroelectricity in these structures is suppressed.

On the other hand, considering the locality principle, one may expect a tendency of gradually arising rumpling of uniform sign to establish. In order to assess the influence of thickness, we increase the RP and Magneli supercells to 26 atomic layers. With increasing length from the interface, the interfacial effects become lees predominant. For the RP structure, the uniformity of rumplings begins to establish from the fifth or sixth layer off the interface.[42] The comeback is rather remarkable in the Magneli supercell, with all but one layers possess rumplings of the same sign, the magnitude of which ranges from 0.02 to 0.07 Å. Further referring to the coherency of the polarization at the upper half and the lower half of a supercell, the long-range characteristic of ferroelectricity is not cancelled by the induced planar defects.

Comparing to the results with unfixed in-plane lattice constant, we find that the epitaxially strained relaxation results do not noticeably differ from that in Table II. The impact of constraining the in-plane constant is small both to the polar FE phase and to the central symmetric PE phase. Take the PE phase, for example, the out-of-plane lattice constant *c*s for both the normal stacking and RP supercells increases by about 0.2% under the epitaxially strained condition while for the Magneli supercell, *c* increases by about 0.8%. Hence the impact of applied strain is more pronounced for the Magneli structure. As is mentioned above, the two adjacent TiO_6 octahedra at the interface seriously influences the final interfacial geometry. Two octahedra get contact by a point at normal stacking, separate by half a unitcell in RP case, and get contact by a sharing edge in Magneli case. In the Magneli situation, epitaxial strain gives compressive stress to the *x* axis while brings tensile stress to the *y* axis of the octahedra.

It is the reason why the Magneli supercell is the most sensitive to the in-plane lattice constant.

B. Interfacial stability

By calculating the work of separation[43,44] of the interfaces, we may reveal the interfacial stability of these structures. There are mainly two popular kinds of methods to determine the work of separation with first-principles calculations: one method accounts for the further relaxation after the separation; the other does not. The former way gives the relaxed work while the latter gives the ideal work of separation by considering only rigid separated parts, without allowing energy lowering by relaxation. By reducing the total energy of the separated parts, allowing further relaxation affects the final W_{sep} slightly. Generally both methods illustrate analogous trend for the comparison among models (for a comparison of rigid and relaxed works of separation, see, e.g., Ref. 44). Calculations here take the latter way to reflect the stability (the ideal work for a "cleavage") of the interface.

The work of separation W_{sep} is given by $W_{sep}=(E_1+E_2-E_{12})/A$, where E_{12}, E_1, and E_2 are the total energy of the supercell, the isolated STO part, and the PTO part, individually. And all the quantities are normalized by the interface area A. Acquired results are 5.29, 2.67, and 4.67 eV for $[PTO]_4/[STO]_4$, RP and Magneli interfaces, respectively. It clearly shows that RP interface has the lowest W_{sep}, indicating weak bonding at the interface, which goes along with the relaxation and interfacial distances results. It can be interpreted by the strong repulsion caused by Sr and Pb cations at the interface. The defect-free interface is the most stable for it keeps the natural perovskite structure at the interface. Unlike the STO/LAO system, Magneli interface is much more stable (nearly 75% higher) than RP interface in STO/PTO system, which is similar to the case in STO/SRO ($SrRuO_3$) system,[37] although these are quite different systems with different physics against PTO system since LAO has a polar interface and SRO is metallic electrode. The stronger stability of RP interface in STO/LAO system can be explained by charge transfer energy cost, considering that SrO-LaO interface is electrically positive while PbO-SrO interface is electrically neutral.

C. Polarization behavior

Here we refer to the polar state of the superlattices, i.e., the FE polarization. In Table I, the polarization along [001] of various superlattices is presented, including that of bulk PTO for comparison. Results from our calculations are given by Berry Phase method[45,46] which has been shown to be in good agreement with electrostatic model.[5,13]Values in parentheses in Table I are for the epitaxially strained supercells, which are very close to those of zero stressed ones.

For the normal stacking case since the in-plane lattice constant under the zero stress condition for the PTO/STO superlattice is almost the same as that for the PTO bulk, the PTO layers are not regarded to suffering applied strain. While under the epitaxially strained condition, due to the lattice mismatch between two materials, tetragonal PTO layers are under a compressive in-plane strain of 0.16%, suppressing the tetragonality c/a ratio of PTO. It has been shown that such misfit strain may slightly increase the polarization of PTO (Ref. 13) while this effect is so tiny that can be ignored in our discussion.

What is noticeable is that the zero-stressed PTO layers in Magneli structure is under a tensile in-plane strain ($\sim$0.3%) along x axis. It was shown that tensile strain will induce in-plane polarization in PTO,[47] which was shown to be important in the analogous PTO/STO superlattice system.[15] However, the magnitude of tensile strain for emerging in-plane polarization should be larger than about 1.1% (from Fig. 2 in Ref. 47), the tensile strain here is much smaller. Hence we do not consider in-plane polarization in our work.

As is implied in the discussion of relaxation and rumpling parameter, FE polarization grossly keeps its direction and magnitude throughout the whole supercell, which is consistent with the previous studies in FE superlattice systems.[13,14] It is further verified by computing the local polarization from the Born effective charge for the ions. It was commonly presumed that the layer polarization is constant in such systems, i.e., $dP/dz=0$. However, none of the superlattices in these works have precisely constant layer polarization. It will be discussed further in the next section.

Both of the two planar-defective superlattices undergo suppression of polarization. Once again, the lack of continuity of Ti-O chains is an important cause of the suppression. It can be also understood in view of the severe repulsion between layers at the interface, expansion of 0.51 and 0.27 Å for RP and Magneli interface, which gives vertically compressive stress to the respective PTO and STO layers. The ferroelectricity is not in the ascendant here also because the scale of polarized rumpling is much smaller than the defect-induced rumpling. Two TiO_2 inserted models have obvious different polarizations. The xy interface also suppresses the FE polarization. It implies that TiO_2 layers at xy interface form a comparatively stable anatase structure, which is nonferroelectric.

As a whole these categories of defects mostly reduce the FE polarization by a certain scale. The xx-type interface are not so stable as the xy one (2.4 eV higher in the total energy) and thus is unpractical, although it gives considerable magnitude in polarization (even larger than that of normal stacking within the PBE functional).

D. Electronic properties

In order to get insight into the electronic properties of the FE superlattice system, we analyze the calculated density of state, as shown in Fig. 4. The calculated band-gap values for normal stacking, RP and Magneli superlattices, and superlattices with xx- and xy-type TiO_2 inserted layers are 1.49 eV, 1.14 eV, 1.20 eV, 0.26 eV, and 1.04 eV, respectively. The valence band edge (VBE) and conduction band edge (CBE) are mainly contributed by the O $2p$ orbital and Ti $3d$ orbital, respectively. The results show that defective interfaces have a narrower bandgap. The RP- and Magneli-type planar defects, perturbing the bonding environment at the interfaces,

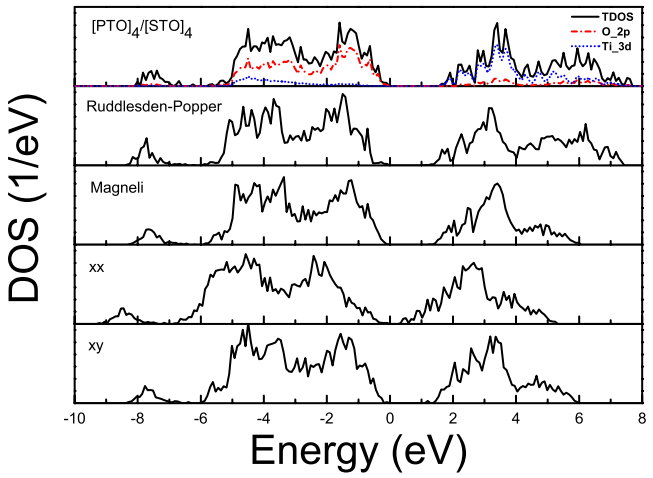

FIG. 4. (Color online) Total density of state of various FE superlattices. The red dash-dotted (blue dotted) line shows the partial density of state contributed by $O_{2p}(Ti_{3d})$ orbital.

slightly reduce the gap by 0.2–0.4 eV. With the TiO_2 adlayer inserted, the interfacial structure is severely disturbed and bandgap becomes much smaller (nearly vanished in xx model). By referencing to the core levels of atoms, we can also see that the gap of xx model reduces by inducing new occupied and unoccupied states at the top of VBE and the bottom of CBE level, respectively, both of which are contributed by the atoms at interfacial TiO_2 layers.

The internal electric field in the normal stacking FE superlattice is estimated by the planar and macroscopic[37,48] average of the electrostatic potential, see Fig. 5. The depolarizing field of FE slab, which does not depend on the thickness of the slab, tends to lift the potential from one side of the slab to the other. Hence the local potential in the PTO and STO layers are sloped[49] rather than flat bottom and top.[37] It can be seen in Fig. 5 that the electric potential in these two materials inclines toward opposite sides. The field in PTO acts as the depolarizing field, however, that in STO cannot be

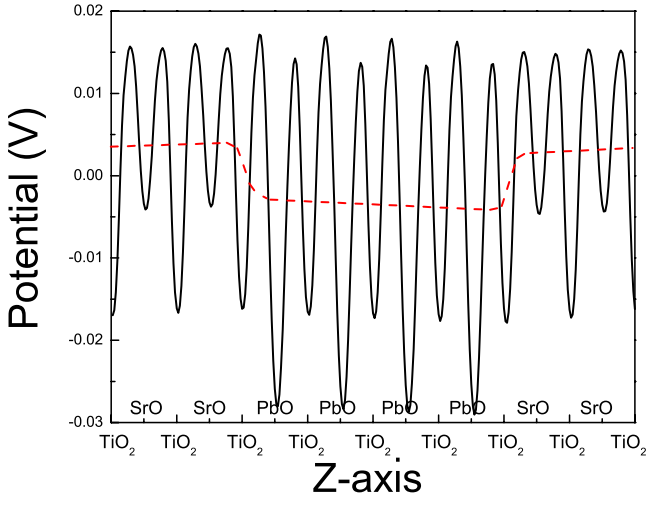

FIG. 5. (Color online) Planar- (black solid) and macroscopic-average (red dashed) of the internal potential of polar $[PTO]_4/[STO]_4$ superlattice

regarded as depolarizing field because its direction is parallel to the polarization direction. As mentioned above, the value dP/dz was always recognized to be zero. Whereas if it is so, the slope of internal field should be of the same sign at both the PTO and STO slabs.

The reason why in first-principles calculation dP/dz is always seems to be zero throughout these superlattices may be that when we calculated the layer-by-layer polarization with Born effective charge, the contributions for oxygen displacements for every local unit cell are usually averaged out,[13,14,41] and the volume is taken as that of the artificial five-atom elementary cells, which is also a mean value. Furthermore, the values of Born-effective charges for atoms are always obtained with bulk materials, which confines its application to superlattices and interfaces to be only qualitative. The variation in P then is probably overlooked with such disposal.

It can be comprehended assuming charge, or effective charge, redistribution occurs at the interfaces. Actually this charge redistribution plays a role of compensation to the FE PTO layers to minimize the electrostatic energy. In this way FE state is ensure to be kept stable. However, STO is semiconducting or insulating layer, and there is no free charge accumulation at the interface to act as screening charge. Thus charge compensation is partially implemented by the bound electrons and hence only very modest.

The effective charge here is interpreted as follows. First of all, the electronegativity of Sr and Pb atom being quite different, 0.95 for Sr and 2.33 for Pb in Pauling units, the electron affinity at either side of the interface is distinct from each other. Then the interfacial unit cell is defined as the interface, see the schematic illustration in Fig. 6(a). Thus the interfacial unit cell is constituted by half a PbO plane, a whole TiO_2 plane, and half a SrO plane (P-T-S). The PTO slab locates between a P-T-S and an S-T-P interface, so does the STO slab. These P-T-S or S-T-P cell possess an unhomogeneous charge distribution inside. In a PE (centrosymmetric) supercell, interfaces on two sides do not yield a mesoscopic electric field across the PTO and STO slab due to symmetry. However, when the supercell is polarized under FE phase transition, the broken symmetry will finally give rise to a mesoscopic electric field. It can be regarded as derivative from the difference of the accumulation of effective charge at both interfaces.

The existence of internal field leads to elaborate structure to the electron states. The energy of state electrons of the TiO_2 layer at the lower interface is lifted up compared to that of the upper layer, with such an offset the total VBE and CBE are contributed by ions on alternative sides. The shift of the LDOS between the upper and lower interface is calculated to be 0.44 eV in $[PTO]_n/[STO]_n$ where the index of period $n=4$ (see, Fig. 7). The shift will increase linearly with increasing index, e.g., for $n=8$, the corresponding value is calculated to be 0.84 eV. Hence it would seem to give rise to the insulator to metal transition (IMT) as the thickness increases when this shift of LDOS exceeds the value of the local band gap. However, this transition is sophistic for some reasons. First, it is hard to occur in PTO/STO system because the internal field is of quite a small magnitude. The electric field here is even smaller than the screened depolarizing field

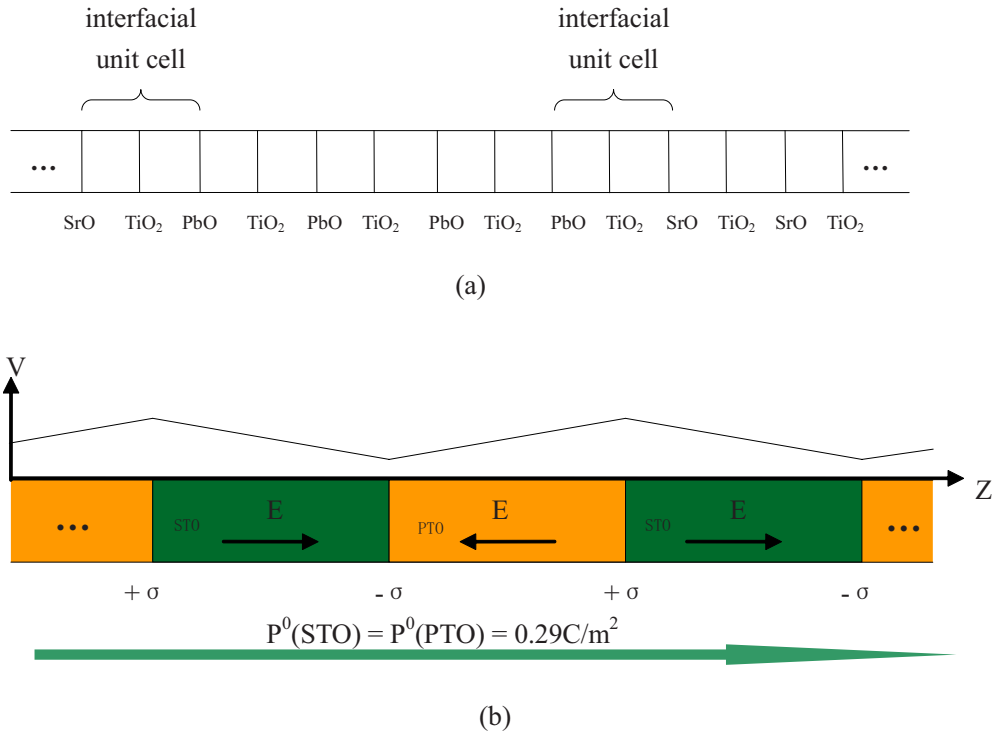

FIG. 6. (Color online) Schematic illustrations for (a) superlattice with S-T-P and P-T-S interfaces, and (b) capacitor plates model for PTO/STO superlattice with interface charge of $\pm\sigma$. V and E are, respectively, the electrostatic potential and electric field arising from the net charge.

in PTO with Pt electrodes in Ref. 49. In order to actualize the IMT, the estimated index n approximates to be 16. It will be even larger if we take into account the underestimation of band gap in first-principles calculations. Moreover it is doubtful whether the linear dependence of the shift of LDOS and the length of repeating period still keeps under such a long-range repetition. Finally and more fundamentally, large FE polarization cannot be stable in metallic materials. If IMT occurs, FE polarization will be reduced due to partial charge back transfer. The internal field will then be suppressed, and the IMT can be restricted as a result. Domain structures are also supposed to emerge to screen the field before the slab reaches the critical thickness.

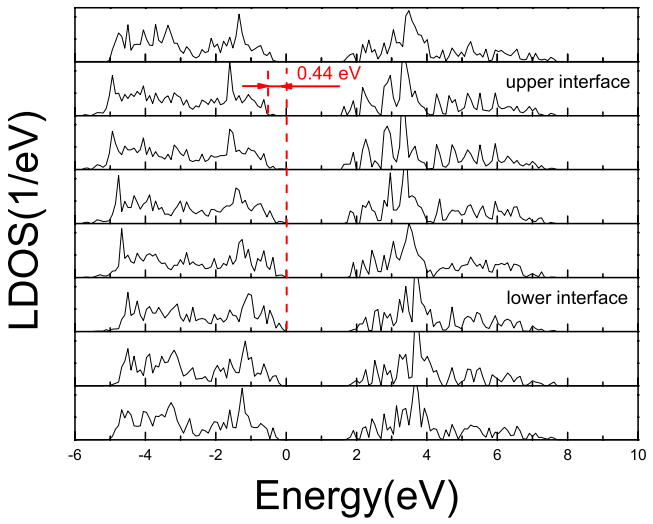

FIG. 7. (Color online) Local density of state of TiO_2 layers in $[PTO]_4/[STO]_4$ supercell.

In addition the superlattice system can be simulated with the capacitor plates model, see Fig. 6(b). Assuming the length for PTO and STO layers being the same, the interfacial charge σ in this simple model can be obtained using the Gauss's law and periodic boundary conditions,

$$\sigma_{net} = \sigma - P_{\mathrm{PTO}} - P_{\mathrm{STO}} = 2\epsilon_0 E, \tag{1}$$

where σ_{net} is the net charge, $P_{\mathrm{PTO(STO)}}$ is the respective polarizations of both materials, ϵ_0 is the dielectric constant of vacuum, and E is the magnitude of the electric field in Fig. 6(b). We have $P = \pm P^0 + \epsilon_0 \chi E$, with the negative sign taken for P^0_{PTO} due to the direction of spontaneous polarization of PTO being reversed to the field. As is discussed above, the FE polarizations for both materials are nearly the same, that is $P^0_e \approx P^0_{\mathrm{STO}} = 0.29\ \mathrm{C/m^2}$, and hence these terms are eliminated in the final expression. Equation (1) can be rewritten,

$$\sigma = \epsilon_0 E(2 + \chi_{\mathrm{PTO}} + \chi_{\mathrm{STO}}). \tag{2}$$

E is found to be $\sim 0.1\ \mathrm{mV/Å}$ from the slope of macroscopic average of internal potential. The susceptibilities are computed as in Ref. 50 with the phonon calculation using the method of linear response.[51] We take $\chi = \chi^{ph}_{33} + \epsilon^{\infty}$, where the phonon contributions obtained are $\chi^{ph}_{33}(\mathrm{PTO}) = 1026$ and $\chi^{ph}_{33}(\mathrm{STO}) = 50$ with such strain and relaxation conditions. The electronic contributions are obtained from calculated bulk quantities, $\epsilon^{\infty}(\mathrm{PTO}) = 7.29$ and $\epsilon^{\infty}(\mathrm{STO}) = 6.39$ (7.24 and 5.18 from literatures[52,53] for comparison). With all these

quantities, we finally get the interfacial charge $\sigma=9.66\times10^{-3}$ C/m^2, or 0.009 electrons per two-dimensional unit cell. It is quite a small value. However, it is unnegligible since its existence derives the zigzag local density and internal potential structures.

IV. CONCLUSIONS

Our calculations of different interfaces in STO/PTO superlattice system show that the interfaces with the normal stacking should be energetically favorable. The interface with RP-type defect is not stable because two cations at the interface exhibit great repulsion and cause severe buckling. Magneli-type interface is energetically more stable. Potential structures with an inserted TiO_2 adlayer by inducing two Magneli defects at the interface are predicted to have a narrower band gap. The xx-type interface enhances FE polarization while it may be energetically unfavorable. Slopelike internal potential in the superlattice is found, which can be explained as a combination phenomena of ferroelectricity and effective charge accumulation at interfaces. This kind of electric potential gives rise to a zigzag local density of states among layers along the vertical direction of the slab, which induces the appearance alternatively between *n*- and *p*-type interfaces in the PTO/STO system alternatively. This is caused by the effective charge located at the interfaces, which is also evaluated.

ACKNOWLEDGMENTS

This work has been supported by NNSFC (under Grants No. 10974081, No. 10774065, and No. 10979017) and NKPBRC (under Grants No. 2006CB921802 and No. 2009CB929500). We are grateful to the High Performance Computing Center of Nanjing University for the award of CPU hours to accomplish this work. The authors thank X. G. Wan, Nanjing University, for his useful discussions.

*xswu@nju.edu.cn

[1] R. A. McKee, F. J. Walker, and M. F. Chisholm, Science **293**, 468 (2001).
[2] M. Dawber, K. M. Rabe, and J.-M. Scott, Rev. Mod. Phys. **77**, 1083 (2005).
[3] R. E. Cohen, Nature (London) **358**, 136 (1992).
[4] J. Junquera and P. Ghosez, Nature (London) **422**, 506 (2003).
[5] M. Dawber, C. Lichtensteiger, M. Cantoni, M. Veithen, P. Ghosez, K. Johnston, K. M. Rabe, and J.-M. Triscone, Phys. Rev. Lett. **95**, 177601 (2005).
[6] E. Bousquet, M. Dawber, N. Stucki, C. Lichtensteiger, P. Hermet, S. Gariglio, J.-M. Triscone, and P. Ghosez, Nature (London) **452**, 732 (2008).
[7] K. Johnston, X. Huang, J. B. Neaton, and K. M. Rabe, Phys. Rev. B **71**, 100103(R) (2005).
[8] Z. Kutnjak, J. Petzelt, and R. Blinc, Nature (London) **441**, 956 (2006).
[9] S. de Lazaro, E. Longo, J. R. Sambrano, and A. Beltran, Surf. Sci. **552**, 149 (2004).
[10] M. Sepliarsky, M. G. Stachiotti, and R. L. Migoni, Phys. Rev. B **72**, 014110 (2005).
[11] J.-M. Zhang, Q. Pang, K.-W. Xu, and V. Ji, Surf. Interface Anal. **40**, 1382 (2008).
[12] T. Shimada, Y. Umeno, and T. Kitamura, Phys. Rev. B **77**, 094105 (2008).
[13] Z. Zhu, B. Wang, H. Wang, Y. Zheng, and Q. K. Li, Solid-State Electron. **50**, 1756 (2006).
[14] S. H. Shah, P. D. Bristowe, A. M. Kolpak, and A. M. Rappe, J. Mater. Sci. **43**, 3750 (2008).
[15] S. M. Nakhmanson and I. Naumov, Phys. Rev. Lett. **104**, 097601 (2010).
[16] S. N. Ruddlesden and P. Popper, Acta Crystallogr. **10**, 538 (1957).
[17] S. N. Ruddlesden and P. Popper, Acta Crystallogr. **11**, 54 (1958).
[18] S. Andersson, B. Collen, U. Kuylenstierna, and A. Magneli, Acta Chem. Scand. (1947-1973) **11**, 1641 (1957).
[19] N. Erdman, K. R. Poeppelmeier, M. Asta, O. Warschkow, D. E. Ellis, and L. D. Marks, Nature (London) **419**, 55 (2002).
[20] R. Herger, P. R. Willmott, O. Bunk, C. M. Schleputz, B. D. Patterson, and B. Delley, Phys. Rev. Lett. **98**, 076102 (2007).
[21] R. I. Eglitis and D. Vanderbilt, Phys. Rev. B **77**, 195408 (2008).
[22] J. Wang, M. Fu, X. Wu, and D. Bai, J. Appl. Phys. **105**, 083526 (2009).
[23] G. Kresse and J. Furthmuller, Comput. Mater. Sci. **6**, 15 (1996).
[24] R. D. King-Smith and D. Vanderbilt, Phys. Rev. B **49**, 5828 (1994).
[25] P. E. Blöchl, Phys. Rev. B **50**, 17953 (1994).
[26] G. Kresse and D. Joubert, Phys. Rev. B **59**, 1758 (1999).
[27] Z. Wu, R. E. Cohen, and D. J. Singh, Phys. Rev. B **70**, 104112 (2004).
[28] Y. Umeno, B. Meyer, C. Elsasser, and P. Gumbsch, Phys. Rev. B **74**, 060101(R) (2006).
[29] D. I. Bilc, R. Orlando, R. Shaltaf, G. M. Rignanese, J. Iniguez, and P. Ghosez, Phys. Rev. B **77**, 165107 (2008).
[30] Z. Wu and R. E. Cohen, Phys. Rev. B **73**, 235116 (2006).
[31] J. P. Perdew, K. Burke, and M. Ernzerhof, Phys. Rev. Lett. **77**, 3865 (1996).
[32] H. J. Monkhorst and J. D. Pack, Phys. Rev. B **13**, 5188 (1976).
[33] O. Nakagawara, M. Kobayashi, Y. Yoshino, Y. Katayama, H. Tabata, and T. Kawai, J. Appl. Phys. **78**, 7226 (1995).
[34] A. M. Glazer and S. A. Mabud, Acta Crystallogr., Sect. B: Struct. Crystallogr. Cryst. Chem. **34**, 1065 (1978).
[35] T. Suzuki and M. Fujimoto, J. Appl. Phys. **89**, 5622 (2001).
[36] C. Jia, J. R. Contreras, J. Schubert, M. Lentzen, U. Poppe, H. Kohlstedt, K. Urban, and R. Waser, J. Cryst. Growth **247**, 381 (2003).
[37] J.-M. Albina, M. Mrovec, B. Meyer, and C. Elsasser, Phys. Rev. B **76**, 165103 (2007).
[38] S. M. Nakhmanson, Phys. Rev. B **78**, 064107 (2008).
[39] J. Padilla and D. Vanderbilt, Phys. Rev. B **56**, 1625 (1997).
[40] M. Stengel, D. Vanderbilt, and N. A. Spaldin, Phys. Rev. B **80**, 224110 (2009).

[41] S. M. Nakhmanson, K. M. Rabe, and D. Vanderbilt, Appl. Phys. Lett. **87**, 102906 (2005).
[42] The uniformly-rumpled layers locate at the middle between two interfaces, five layers from one interface and six layers from the other. We do not show the full data of this since the supercells is too large.
[43] A. Hashibon, C. Elsasser, Y. Mishin, and P. Gumbsch, Phys. Rev. B **76**, 245434 (2007).
[44] A. Hashibon, C. Elsasser, and M. Ruhle, Acta Mater. **53**, 5323 (2005).
[45] R. D. King-Smith and D. Vanderbilt, Phys. Rev. B **47**, 1651 (1993).
[46] D. Vanderbilt and R. D. King-Smith, Phys. Rev. B **48**, 4442 (1993).
[47] C. Bungaro and K. M. Rabe, Phys. Rev. B **69**, 184101 (2004).
[48] J. Junquera, M. H. Cohen, and K. M. Rabe, J. Phys.: Condens. Matter **19**, 213203 (2007).
[49] N. Sai, A. M. Kolpak, and A. M. Rappe, Phys. Rev. B **72**, 020101(R) (2005).
[50] N. C. Bristowe, E. Artacho, and P. B. Littlewood, Phys. Rev. B **80**, 045425 (2009).
[51] S. Baroni, S. de Gironcoli, A. D. Corso, and P. Giannozzi, Rev. Mod. Phys. **73**, 515 (2001).
[52] L. Yu, V. Ranjan, M. B. Nardelli, and J. Bernholc, Phys. Rev. B **80**, 165432 (2009).
[53] W. Zhong, R. D. King-Smith, and D. Vanderbilt, Phys. Rev. Lett. **72**, 3618 (1994).